$$\frac{(U_1 + U_5)}{\text{trace}[Q]} = U_1^* + U_5^* = \frac{1}{2} \tag{1.9}$$

Where U_1^* and U_5^* are the trace normalized invariants U_1 and U_5, respectively.

1.3 Trace and other invariants

Typical properties of 15 carbon/epoxy composite plies in terms of engineering constants, plane-stress components $[Q]$, their respective trace, and trace-normalized engineering constants are listed in Table 1.3.

Table 1.3. Stiffness components, trace, and normalized engineering constants for CFRP leading to universal stiffness values.

	Ply engineering constants				Plane-stress stiff matrix				Trace	Trace-normalized		
15 Ply material	E_x	E_y	E_s	ν_x	Q_{xx}	Q_{yy}	Q_{xy}	Q_{ss}	Trace	E_x^*	E_y^*	E_s^*
IM6/epoxy	203	11.2	8.4	0.32	204	11.3	3.6	8.4	232	0.874	0.048	0.036
IM7/977-3	191	9.9	7.8	0.35	192	10.0	3.5	7.8	218	0.877	0.046	0.036
T300/5208	181	10.3	7.2	0.28	182	10.3	2.9	7.2	206	0.877	0.050	0.035
IM7/MTM45	175	8.2	5.5	0.33	176	8.2	2.7	5.5	195	0.897	0.042	0.028
T800/Cytec	162	9.0	5.0	0.40	163	9.1	3.6	5.0	183	0.888	0.049	0.027
IM7/8552	159	9.0	5.5	0.32	160	9.0	2.9	5.5	180	0.884	0.050	0.031
T800S/3900	151	8.2	4.0	0.33	152	8.2	2.7	4.0	168	0.898	0.049	0.024
T300/F934	148	9.7	4.6	0.30	149	9.7	2.9	4.6	168	0.883	0.058	0.027
T700 C-Ply 64	141	9.3	5.8	0.30	142	9.4	2.8	5.8	163	0.866	0.057	0.036
AS4/H3501	138	9.0	7.1	0.30	139	9.0	2.7	7.1	162	0.852	0.055	0.044
T650/epoxy	139	9.4	5.5	0.32	140	9.5	3.0	5.5	160	0.866	0.059	0.034
T4708/MR60H	142	7.7	3.8	0.34	143	7.8	2.6	3.8	158	0.897	0.049	0.024
T700/2510	126	8.4	4.2	0.31	127	8.5	2.6	4.2	144	0.877	0.058	0.029
AS4/MTM45	127	7.9	3.6	0.30	128	8.0	2.4	3.6	143	0.889	0.055	0.025
T700 C-Ply 55	121	8.0	4.7	0.30	122	8.0	2.4	4.7	139	0.869	0.057	0.034
					Trace = $Q_{xx} + Q_{yy} + 2Q_{ss}$							
Average = Universal				0.320					1.000	0.880	0.052	0.031
Std dev				0.029						0.013	0.005	0.006

The average and standard deviations for the normalized engineering constants are shown in the bottom two rows of Table 1.3. These average values are the universal ply constants (master ply) for carbon fiber reinforced polymers. The average components of $[Q]$ are shown in Equation (1.10).

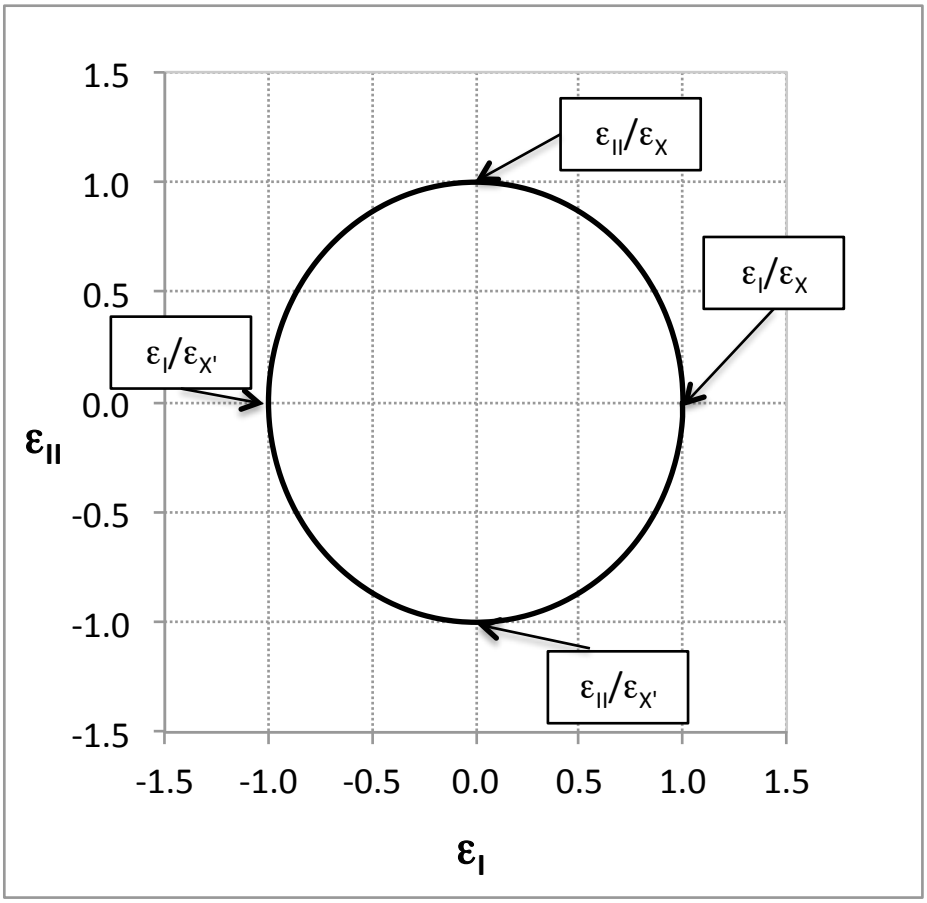

Figure 2.28. Unit circle failure envelope.

Unit circle failure envelopes can be derived for any CFRP laminate if the anchor points in Figure 2.28 are multiplied by the respective strains-to-failure ε_X and $\varepsilon_{X'}$. In Figure 2.29, failure envelopes for six CRPFs based on the unit circle and on LPF omni envelopes are shown for purposes of comparison.

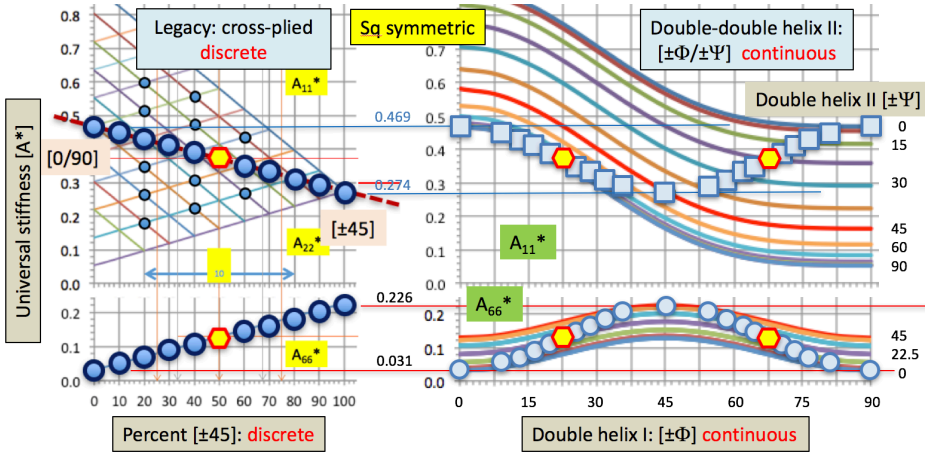

	A	B	C	D	E	F	G	H	I	J	K	L
184	%[±45]	0	10	20	30	40	50	60	70	80	90	100
185	A11*	0.468	0.449	0.430	0.410	0.391	0.371	0.352	0.332	0.313	0.293	0.274
186	A66*	0.032	0.051	0.070	0.090	0.109	0.129	0.148	0.168	0.187	0.207	0.226
187	Helix PHI	0.0	9.0	13.4	16.5	19.7	22.5	25.4	28.2	31.7	35.7	45.0
188	Helix PSI	90.0	81.0	76.6	73.5	70.3	67.5	64.6	61.8	58.3	54.3	45.0
189	Helix PHI	45.0	54.3	58.3	61.8	64.6	67.5	70.3	73.5	76.6	81.0	90.0
190	Helix PSI	45.0	36.0	31.6	28.5	25.3	22.5	19.6	16.8	13.3	9.3	0.0

Figure 3.28. Replacement of legacy laminates (left) by double-double I-II (right). Such replacement is exact. Numerical values are shown in the table for both helix I and II.

The 20 other members of the legacy family (29 minus 9 square symmetric) can be matched to various degree of accuracy by members of the double-double family. The results are shown in Figure 3.29. There are 3 blocks of laminates, as defined by the angle of helix 2 in ψ in the last row: 22.5, 45 and 67.5. Within each block, the angle for helix 1 φ is listed in ascending order. These two angles are laminates from the double-double helix 1 and 2 that would come close to the legacy laminates. The stiffness components for the legacy are listed first in rows 146-148. The best-matched double-double are shown in rows 150-152. In the middle block where ψ = 45 the match is exact, as seen in the last two figures. For the remaining 2 blocks where ψ = 22.5 and 67.5, the match is good for most laminates except for the last 4 or 5 laminates.

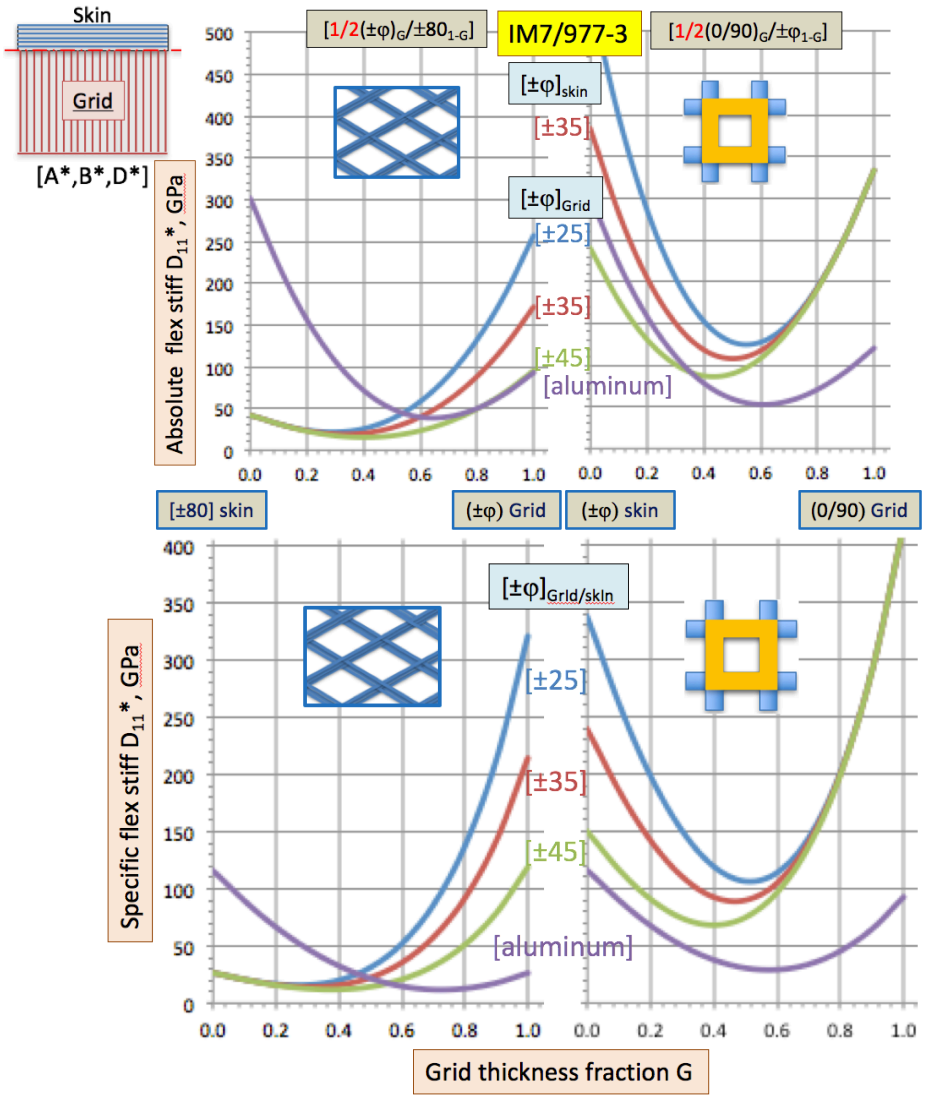

Figure 4.16. Absolute and specific flexural stiffness of three bi-ax grid and one skin, and one square-grid and three bi-ax skins.

From Figure 4.16, aluminum grid and skin is hard to justify from the flexural stiffness point of view. Solid laminate (G = 0) gives the highest D_{11}^{*} for all grid thickness fractions. Composite grids, on the other hand, are very effective to increase flexural rigidity. Such feature can increase buckling loads and flexural frequencies and is not possible with aluminum grids, with or without skin.

In addition to the triaxial $[0/\pm45/0]_s$ layup, other layups such as QI $[0/\pm45/90]_s$ (or $[\pi/4]_s$), another triaxial layup $[0/\pm25/0]_s$, two biaxial layups $[\pm12.5]_s$ and $[\pm22.5]_s$ were also considered. Figure 5.5 (a) shows the optimal thickness profile of the cantilever beam with these layups under the Load case #1. As a reference, the optimal weight of aluminum metal was also obtained. The QI layup requires the thickest profile because of [90] ply, whose fibers are oriented in the perpendicular to the beam's length direction. The biaxial $[\pm12.5]_s$ layup requires the thinnest profile because the fiber orientations are closest to the beam's length direction. The triaxial $[0/\pm25/0]_s$ results in the second least thickness profile. It is interesting to note that the triaxial $[0/\pm45/0]_s$ results in very similar profile as the biaxial $[\pm22.5]_s$, which are very close to the aluminum.

Figure 5.5 (b) shows the weight of the five laminate layups and the aluminum against the power exponents (n) of the cosine profile function in Equation (5.1). Red circles indicate the minimal weight and the corresponding n. As figure shows, n happens to be 0.75 for all five laminates as well as the aluminum. Therefore, the n values for the optimal weight are relatively insensitive to lamination under this concentrated loading condition. It is interesting to note that $[\pi/4]$ QI laminate has a thicker profile than the aluminum, but because of the significantly lower density of composites ($1.6\ g/cm^3$) than that of aluminum ($2.7\ g/cm^3$), the weight saving of using the composites is substantial compared with the aluminum.

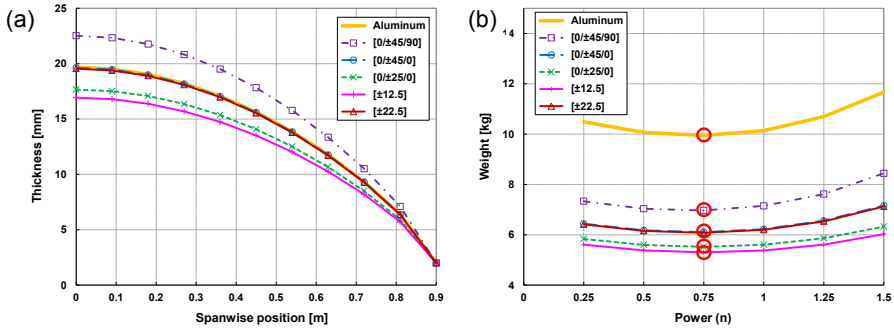

Figure 5.5. (a) Optimal thickness profiles of a cantilever beam of T700/epoxy C-Ply 55 with a triaxial $[0/\pm45/0]_s$ layup under Load case #1 in Figure 5.1 (a). (b) Weight of the five laminate layups and the aluminum against the power exponents (n) of the cosine profile function in Equation (5.1).

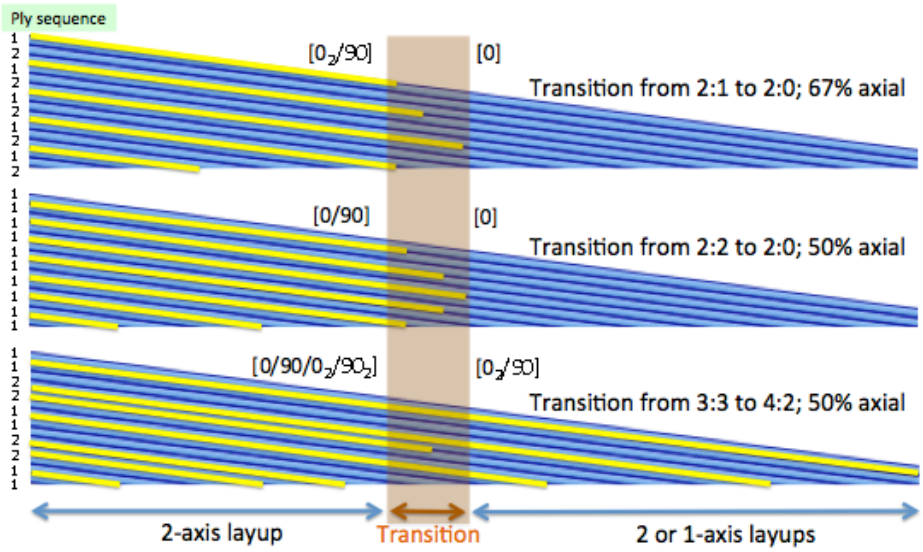

Figure 6.7. Transition between different layup ratios.

Figure 6.8 shows a possible solution for the transition between 3 zones. The guidelines remain the same; i.e., one ply is dropped per sub-laminate, maintaining the axial tape continuous from the root to the tip. With these principles, it is possible to have many zones with each zone with an increment of one ply per sub-laminate. There is, however, some limit at which homogenization becomes difficult to maintain.

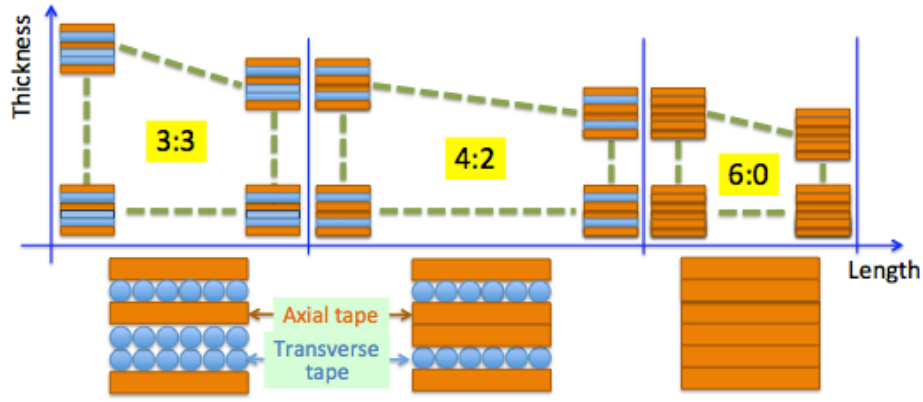

Figure 6.8. Example of a layup transition between 3 zones.

Tapering in two directions can follow the same strategy. Homogeneity is still a helpful feature; whether it is a ply drop or build up, the patch

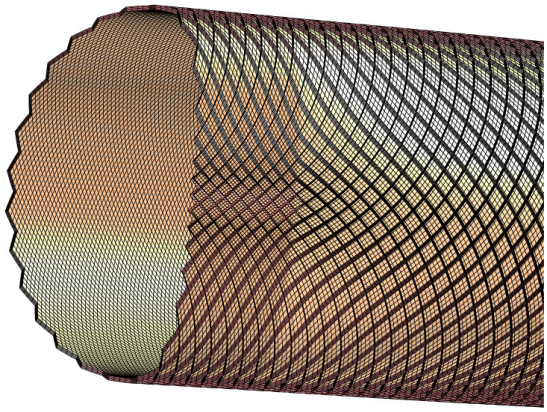

Figure 7.19. Tail Where Fuselage Changes Shape.

At some point, the nose of the fuselage (Figure 7.20) can be completed using a panel. Care is needed so that the tangents of the lattice structure on the fuselage match the tangents of the lattice structure of the panel where they meet.

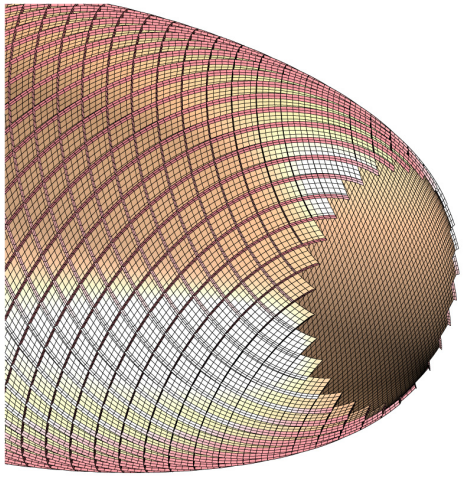

Figure 7.20. Incomplete Nose of the Fuselage.

The door and windows of this FEM are ideal in dimensions and locations to cause the least disturbance to the lattice structure pattern (Figure 7.21). It is unlikely that this can happen in a real design.